

[Click here to view linked References](#)

1 SEDIMENTS, SEC 3 • HILLSLOPE AND RIVER BASIN SEDIMENT DYNAMICS •

2 RESEARCH ARTICLE

3

4 **Coupling hysteresis analysis with sediment and hydrological connectivity in three**
5 **agricultural catchments in Navarre, Spain**

6
7
8 **Saskia D. Keesstra^{1,2} • Jason Davis³ • Rens Hein Masselink³ • Javier Casali⁴ • Edwin**
9 **T.H.M. Peeters⁵ • Roel Dijkma⁶**

10 ¹Team Soil Water and Land Use, Wageningen Environmental Research, Wageningen UR
11 Postal address: P.O. Box 47, 6700 AA Wageningen, The Netherlands

12 ²Civil, Surveying and Environmental Engineering, The University of Newcastle, Callaghan
13 2308, Australia.

14 ³Soil Physics and Land Management Group, Wageningen University, Droevendaalsesteeg 4,
15 6708 PB. Wageningen, The Netherlands

16 ⁴Department of Engineering, Public University of Navarre, Campus Arrosadía, 31006,
17 Pamplona, Spain

18 ⁵Aquatic Ecology and Water Quality Management Group, Wageningen University,
19 Droevendaalsesteeg 4, 6708 PB. Wageningen, The Netherlands

20 ⁶Department of Hydrology and Quantitative Water Management, Wageningen University,
21 Droevendaalsesteeg 4, 6708PB Wageningen, Netherlands

22
23
24 ✉ Saskia D. Keesstra

25 saskia.keesstra@wur.nl

27 **Abstract**

28 **Purpose:** Rain storm events mobilise large proportions of fine sediments in catchment systems.
29 Sediment from agricultural catchments are often adsorbed by nutrients, heavy metals and other
30 (in)organic pollutants that may impact downstream environments. To mitigate erosion,
31 sediment transport and associated pollutant transport it is crucial to know the origin of the
32 sediment that is found in the drainage system and, therefore, it is important to understand
33 catchment sediment dynamics throughout the continuity of runoff events.

34 **Materials and methods:** To assess the impact of the state of a catchment on the transport of
35 fine suspended sediment to catchment outlets an algorithm has been developed which classifies
36 rain storm events into simple (clockwise, counter-clockwise) and compound (figure-of-eight;
37 complex) events. This algorithm is the first tool that uses all available discharge and suspended
38 sediment data and analyses these data automatically. A total of 797 runoff events from three
39 experimental watersheds in Navarre (Spain) were analysed with the help of long-term, high
40 resolution discharge and sediment data that was collected between 2000-2014.

41 **Results and discussion:** Morphological complexity and in-stream vegetation structures acted
42 as disconnecting landscape features which caused storage of sediment along the transport
43 cascade. The occurrence of sediment storage along transport paths was therefore responsible
44 for clockwise hysteresis due to the availability of in-stream sediment which could cause the
45 “first flush” affect. Conversely, the catchment with steeper channel gradients and a lower
46 stream density showed much more counter-clockwise hysteresis due to better downstream and
47 lateral surface hydrological connectivity. In this research hydrological connectivity is defines
48 as the actual and potential transfer paths in a catchment. The classification of event SSC-Q
49 hysteresis provided a seasonal benchmark value to which catchment managers can compare
50 runoff events in order to understand the origin and locations of suspended sediment in the

51 catchment.

52 **Conclusions:** A new algorithm uses all available discharge and suspended sediment data to
53 assess catchment sediment dynamics. From these analysis, the catchment connectivity can be
54 assessed which is useful to develop catchment land management.

56 **Keywords** Headwater catchment • Hydrological event • Hysteresis • Sediment connectivity •
57 Sediment dynamics

58

59

60 **1 Introduction**

1
2
3
4 61 Increased sediment loads, adsorbed with nutrients, heavy metals and other organic and
5
6 62 inorganic pollutants, impact downstream aquatic ecological environments (Owens and Walling
7
8 63 2002; Bilotta and Brazie 2008; Bird et al. 2010; Kjelland et al. 2015; Song et al. 2011). In
9
10 64 Mediterranean areas, soil erosion by water is particularly problematic due to the climatic,
11
12 65 pedological and geomorphological conditions (Cerdan et al. 2010; García-Ruiz et al. 2013).
13
14 66 Long term, high temporally resolute data on precipitation, runoff and water turbidity have
15
16 67 provided the data to study trends in precipitation, runoff and suspended sediment production
17
18 68 (eg. Casali et al. 2008). However, when flow and sediment measurements are confined to
19
20 69 catchment outlet, it has been proven to be difficult to consistently define relationships between
21
22 70 runoff data and the physical processes occurring at the catchment scale (Stubblefield et al. 2007)
23
24 71 which are known to be conditioned by topography, infiltration dynamics, climate, channel
25
26 72 pattern, vegetation, land use and soil properties (Roehl 1962). Based on initial catchment
27
28 73 conditions such as soil moisture, vegetation density, soil erodibility, and (dis)connective
29
30 74 landscape features, sediment production, transfer and storage may be controlled by all parts of
31
32 75 the landscape (Bracken et al. 2015; Cerdà et al. 2018; Parsons et al. 2006; Wainwright et al.
33
34 76 2011). Subsequently, each location in the catchment has a temporally dynamic influence on
35
36 77 both discharge (Q) and suspended sediment concentration (SSC) measured at the outlet.
37
38 78 Hydrograph and suspended sediment time-series analysis have revealed patterns from which
39
40 79 the activation and location of runoff generation and sediment transport processes can be inferred
41
42 80 by classifying hydrological events based on the disparity between the time-to-peak of the
43
44 81 hydrograph and sediment time series.
45
46
47
48
49
50
51
52
53
54
55

56 82 Suspended sediment hysteresis is a term that describes the nonlinear relationship
57
58 83 between SSC and Q during a discharge wave (Klein 1984; Gentile et al. 2010). The array of
59
60
61
62
63
64
65

1
2
3
4
5
6
7
8
9
10
11
12
13
14
15
16
17
18
19
20
21
22
23
24
25
26
27
28
29
30
31
32
33
34
35
36
37
38
39
40
41
42
43
44
45
46
47
48
49
50
51
52
53
54
55
56
57
58
59
60
61
62
63
64
65

84 coordinate points generated by plotting SSC vs. Q through time forms a loop figure (hysteresis
85 loop) whose size, direction and shape reflect the lag in response between SSC and Q (Seeger et
86 al. 2004). This loop figure has been studied using a technique called hysteresis analysis, in
87 which the type and location of physical processes leading to runoff generation and sediment
88 transport are hypothesised to be explanatory factors for the event loop direction and shape (Gao
89 and Josefson 2012; Aich et al. 2014). SSC-Q hysteresis loop examination has thereby allowed
90 for the inferencing of major sediment source areas which are regarded to contribute to sediment
91 transport cascade in catchments (Keesstra et al. 2009; Ziegler et al. 2014). Clockwise loops
92 (CW; with Q on the x-axis and SSC on the y-axis) result from the main SSC peak pre-empting
93 Q peak. In terms of process, this type of curve indicates that sediment is primarily originated
94 from, in or nearby stream channels in the lower part of the catchment (Seeger et al. 2004). It
95 signals the flushing of highly erodible sediment which was deposited from up-catchment
96 locations during prior storm events (Jansson 2002; Wotling and Bouvier 2002; Rovira and
97 Batalla 2006; Gao and Pasternack 2007; Gao and Josefson 2012). Counter-clockwise (CCW)
98 loops result from Q peaking before the SSC. CCW loops may signal distal sediment supply,
99 delayed in-channel sediment resuspension caused by the late break-up of biofilms, in-channel
100 (bank erosion) sediment sources, or intra-storm variable rainfall patterns (Lawler et al. 2006;
101 Lopez-Tarazon et al. 2009; Mano et al. 2009). A more complex figure-eight loop results from
102 secondary peaks in Q or SSC. This type of loop could signal intra-catchment transport of
103 suspended sediment of heterogeneous sizes (Smith and Dragovich 2009) or a combination of
104 different runoff generation processes (Zabaleta et al. 2007).

105 Insofar as it describes catchment runoff and sediment dynamics, hysteresis analysis has
106 evolved from a qualitative classification system into a data-intensive, quantitative technique. In
107 observing single flood events, Williams (1989) and Klein (1984) provided qualitative
108 explanations of the hysteresis loop phenomenon. Subsequent studies in headwater catchments

109 classified events by the loop type (eg. Regüés et al. 2000) and linked event loop types to
110 observed physical processes. However, most of these studies lacked quantitative data which
111 could consistently explain loop directions using statistical models and were unable definitively
112 elaborate on the factors controlling runoff generation. Seeger et al. (2004), in a year-long study
113 in the Central Spanish Pyrenees, not only classified storm events by loop type, but also applied
114 a multivariate analysis in the form of a canonical discriminant analysis to resolve and isolate
115 the combinations of initial physical conditions, such as soil moisture content and antecedent
116 precipitation indices, and ultimately link them to classified loop types. Other studies developed
117 hysteresis indexes which could systemically classify loop direction (the hysteresis index, HI)
118 (Langlois et al. 2005; Lawler et al. 2006; Lloyd et al. 2016), and thus made it possible for
119 quantitative, comparative studies both within and across multiple catchments. In a comparative
120 catchment study, Sherriff et al. (2015) applied a principal component analysis in conjunction
121 with the HI metric to graphically and analytically explain the various factors influencing
122 catchment sediment dynamics.

123 SSC-Q hysteresis analysis can play a role in explaining catchment sediment dynamics
124 under conditions of full data inclusion and use of robust loop analysis methods (Sith et al. 2017).
125 However, further improvements can be made which can fully automate the procedure for loop
126 direction and event type classification. Additional knowledge can be garnered by increasing the
127 relevant data inputs and employing multivariate statistical models which can link event types
128 to a complex set of explanatory data on initial catchment conditions as well as discharge and
129 precipitation variables (Lloyd et al. 2016). The combination of these techniques could greatly
130 improve the understanding of event sediment dynamics by isolating the most important and
131 explanatory event and climatic variables. This presents an opportunity for geomorphological
132 understanding and sediment production in headwater catchments. Therefore, the main aim of
133 this research is to assess the runoff and erosion dynamics in three small Mediterranean

134 catchments (area < 6 km²) by classifying runoff events by the type of hysteresis and linking these
135 groups to the respective catchment characteristic data and event runoff variables. From this
136 analysis the application potential and robustness of this new methodology was assessed.

137

138 2 Materials and methods

139 2.1 Study areas

140 The data in this study come from three catchments in the Navarre region, in Northern
141 Spain (Fig. 1). They are part of a network of experimental research catchments instituted to
142 assess erosion, nutrient transport and hydrological processes within agricultural and semi-
143 natural landscapes (Casalí et al. 2010; Masselink et al. 2016). Catchments were selected based
144 on data availability as well as due to the major differences in land use and cover (Masselink et
145 al. 2016). This made it possible to assess the relevance of different environmental variables on
146 runoff and sediment production. The Latxaga (2.07 km²) and La Tejería (1.69 km²) catchments'
147 land use is dominated by rain-fed agricultural fields (90%) mostly covered with winter wheat
148 (*Triticum aestivum*), barley (*Hordeum vulgare*) and sometimes legumes (*Vicia faba* L. and
149 *Pisum sativum* L.) or sunflower (*Helianthus annuus* L.). However, the stream beds and banks
150 within the La Tejería watershed are poorly vegetated, which enhances the occurrence of bank
151 erosion processes. The Oskotz (5.05 km²) experimental catchment contains nearly 100% forest
152 cover mainly composed of *Fagus sylvatica*, *Quercus pyrenaica* and *Pinus* spp. It is more humid
153 and has a lower runoff coefficient (Casalí et al. 2012) than both agricultural catchments. The
154 Latxaga and La Tejería watersheds both have humid sub-Mediterranean climates, with average
155 annual precipitations of 835 and 725 mm, distributed over 95-100 and 105 rainfall days and
156 average annual temperatures of 12°C and 13°C, respectively. Geologically, these two
157 catchments are underlined by clay marls and grey marls. La Tejería contains sandstones of
158 continental facies. Because of the soft nature of the lithology the sediment yield at the outlet of

159 the catchments consists mainly of suspended sediment. Almost all coarser material has been
160 broken into small sized particles before reaching the outlet of the catchments. Oskotz watershed
161 has a sub-Atlantic climate, with an average annual precipitation of 1242 mm, distributed over
162 130 rainfall days, and an average annual temperature of 12 °C. Detailed climate and catchment
163 environmental properties are shown in Table 1.

2.2 Data collection and data treatment

166 Rainfall was recorded using a tipping bucket device with 0.2 mm resolution with every
167 tip of the device. Additionally, each catchment had at the watershed outlet one hydrology station
168 from which water level (mm) and turbidity (NTU) were recorded every 10 minutes. The
169 discharge measurement device consisted of a triangular profile flat-V weir which allowed
170 sediment to pass the control section; discharge ($\text{m}^3 \text{s}^{-1}$) was calculated from water level data
171 which was gathered using a pressure probe and this was verified with a direct measurement
172 propeller-type current meter and triangular and rectangular sharp-crested weirs. To isolate
173 effects of total rainfall, intensity and duration, a rainfall event erosivity index based on kinetic
174 energy (KE; $\text{MJ ha}^{-1} \text{mm}^{-1}$) of the event precipitation was derived (Morgan 2005). Kinetic
175 energy was calculated according to Cerro et al. (1998). The empirical relationship for KE was
176 based on rain drop size distributions and was derived from regions of similar climatic
177 conditions. Given climatic similarities, the relationship was seen as most representative for the
178 three catchments in this study. Thus, kinetic energy was calculated as follows (Cerro et al.
179 1998):

$$KE = 0.384 * (1 - .54e^{-0.029*I_{60}}) \quad (1)$$

181 Where: I_{60} is the 60-minute rainfall intensity (mm h^{-1}). An event's total kinetic energy was
182 calculated from:

$$KE_{total} = \sum_{t=0}^{Dur} E_t * P_{total} \quad (2)$$

184 Where: t was the time step, E_t was the kinetic energy for each time step and P_{total} was the total
1 rainfall received at time step t . Finally, the EI_{30} was calculated as:

$$EI_{30} = KE_{total} * I_{30} \quad (3)$$

187 Where: I_{30} was the maximum 30-minute rainfall intensity in $mm\ h^{-1}$. For I_{60} intensities above
188 $76\ mm\ h^{-1}$, a maximum I_{60} was used according to (Brown and Foster 1987). The Antecedent
189 Precipitation Index (Linsley and Kohler 1951) was used as a surrogate of soil moisture in this
190 study:

$$API = \sum_{t=0}^i P_t * k^{-1} \quad (4)$$

192 Where: API is Antecedent Precipitation Index (mm), P_t the precipitation on day t (mm), k a
193 calibration factor and t is the number of days before $t=0$. The model for antecedent precipitation
194 was calibrated according to Masselink et al. (2016). Finally, changes in vegetation cover were
195 captured using the Normalised Difference Vegetation Index (NDVI; Dash et al. 2007) and it
196 was used in this study as an indicator for crop maturity and vegetation growth. It was calculated
197 using satellite imagery as:

$$NDVI = \frac{NIR-RED}{NIR+RED} \quad (5)$$

199 Where: NDVI is the Normalised Difference Vegetation Index, NIR the top of atmosphere
200 reflectance in the near infrared wavelength bands and RED the top of the atmosphere
201 reflectance in the red wavelength band (Masselink et al. 2016).

2.3 Storm event separation and hysteresis index calculation

204 Base flow was separated from event (quick) flow by applying a low-pass, recursive
205 digital filtering algorithm to the continuous hydrograph time series according to Eckhardt
206 (2005). The filter considers an exponential base flow recession during periods without
207 groundwater recharge. The separation method requires two parameters: a recession constant, or
208 filtering parameter (a) and a base flow index maximum (BFI_{max}). Recession analysis

209 determined the filtering parameter by constructing a master recession curve and using the
 1 matching strip method (e.g. Nathan and McMahon 1990). BFI_{max} was determined using an
 2 210
 3 empirically derived value which corresponded to classes of catchments containing hydrological
 4 211
 5 and hydrogeological characteristics (Table 2).
 6 212
 7
 8

9 213 An analytic definition for a runoff event allowed for a consistent definition of an ‘event’
 10 over the time period. This made it possible to compare across catchments and between storms.
 11 214
 12 A storm was defined as a 10% rise in quick flow above base flow. Base flow was calculated
 13 215
 14 using the Local Minimum Method (Sloto and Krouse 1996). Each event ended when quick flow
 15 216
 16 dropped below the calculated base flow. Consequently, it was possible to have runoff events
 17 217
 18 with multiple peaks if quick flow stayed greater than base flow. To remove the influence of
 19 218
 20 initial base flow conditions on the HI calculation – in order to focus on the relative changes in
 21 219
 22 each variable – the turbidity and quick flow event time-series for quick were normalized
 23 220
 24 according to the following equations from Lloyd et al. (2015):
 25 221
 26
 27
 28
 29
 30

$$31 \text{ 222 } \textit{Normalized } Q_i = \frac{Q_i - Q_{min}}{Q_{max} - Q_{min}} \quad (5)$$

$$32 \text{ 223 } \textit{Normalized } T_i = \frac{T_i - T_{min}}{T_{max} - T_{min}} \quad (6)$$

33
 34
 35 224 Where: Q_i/T_i is the discharge ($l s^{-1}$)/turbidity(NTU) at time step i , Q_{min}/T_{min} is the minimum
 36 storm parameter value and Q_{max}/T_{max} is the maximum storm parameter value. The hysteresis
 37 225
 38 index was then calculated as:
 39 226
 40
 41
 42

$$43 \text{ 227 } HI = T_{RL_{Q_i}} - T_{FL_{Q_i}} \quad (7)$$

44
 45 228 Where: HI is the index at percentile i of the discharge (Q), $T_{RL_{Q_i}}$ is the turbidity value on the
 46 rising limb at percentile i of Q and $T_{FL_{Q_i}}$ is the turbidity value at the equivalent point in
 47 229
 48 discharge on the falling limb. The percentiles of discharge (Q_i) were defined by:
 49 230
 50
 51
 52

$$53 \text{ 231 } Q_i = k(Q_{max} - Q_{min}) + Q_{min} \quad (8)$$

54
 55 232 Where: Q_{max} is the peak discharge ($l s^{-1}$), Q_{min} is the discharge at the start ($l s^{-1}$) of the event and
 56
 57 k is the point along the loop where the calculation is being made. The index was calculated at
 58 233
 59
 60
 61
 62
 63
 64
 65

234 every 5% of the discharge, making $k = 0.05, 0.10...1.0$ and always produced an HI value
235 between -1 and 1. The sign indicates clockwise versus counter clockwise and the size of the
236 index indicates the strength of the hysteresis, or the width of the loop for the given k discharge
237 range being measured. Each event thus contained an array of HI values, from which the average
238 HI was calculated by taking the average of the array values (Lloyd et al. 2015). Figure 2 shows
239 a model example of CW and CCW events. Time-series curves are identical but are separated
240 slightly in time which produces the hysteresis curve.

241 To characterize the catchments in an objective way we have calculated two indices: the
242 Gravelius Index and the shape factor. The Gravelius index (K_c) has been defined as:

$$244 \quad K_c = 0.28P/A^{0.5}$$

245
246 Where P is the catchment perimeter (m) and A the area (m^2). A perfect circular catchment would
247 have a K_c equal to 1 (Bendjoudi and Hubert, 2002) “In order to characterize the morphology
248 of the watersheds, two indices (Gravelius Index and shape factor) were used.

249 The shape factor, K_f has been defined by Monsalve Saenz (1999) as:

$$251 \quad K_f = A/L^2$$

252
253 Where P is the catchment parameter and L is the maximum length along the main stream from
254 the catchment outlet to the most distant ridge on the drainage divide.

258 **2.4 Event type classification**

259 While the event average HI was descriptive of the general behaviour of the event

260 hydrograph and turbidity time series, it failed to account for intra-storm changes in loop
261 direction, especially mid-storm loop direction reversals. Often events begin as a simple
262 hysteresis events (CW; CCW) and thereafter, due to late peaks or drops in either discharge or
263 turbidity, appear as a figure-of-eight or complex loop. An event might begin as a simple CW
264 loop due to an early turbidity response relative to discharge. Low magnitude spikes in either
265 the discharge or turbidity curves would ensure the loop remains CW. If, however, a large spike
266 in turbidity were to occur on the falling limb of the event's hydrograph, the loop would more
267 likely resemble a figure-of-eight pattern. To capture these intra-storm periodic differences in
268 the sign of HI, we developed a classification algorithm which differentiated between simple
269 and complex events while still maintaining the composite loop directions from each time period,
270 especially the starting and ending loop directions. To do this, we subdivided the event HI array
271 into four equal time periods then computed the average HI for each quartile. An HI quartile was
272 considered CW where $HI > 0$ and CCW where $HI < 0$. We then passed this sequence of values
273 through an function which, based on these sign of the HI in the given range, classified each
274 storm into one of four types (Table 3).

2.5 Statistical analyses and procedures to determine event type controls

277 A number of statistical analysis procedures were performed to investigate controls on
278 hydrological response and event sediment dynamics in each watershed over the course of the
279 study. All variable values were considered as samples from a population. Thus, the central limit
280 theorem was assumed. One-way ANOVA was performed to infer significant differences
281 between sampled event storm variables. When more than two groups were incorporated into an
282 ANOVA and significant variation was found in the model, a Tukey post-hoc test was conducted
283 with $\alpha=0.01$. In some cases, the sample size of the complex and figure-of-eight events was not
284 large enough to include these events in the analysis. The sign of HI was then used to divide the

285 groups into two categories, CW with $HI > 0$ or CCW with $HI < 0$. A one-tailed heterogeneous t-
286 test for variance was then applied to confirm the presence of significant differences between
287 the sampled variable. Finally, for each catchment, canonical variate analysis (CVA) was
288 performed with the Canoco-5 software package (Ter Braak and Smilauer 2012) with the event
289 types as groups and with the variables described in Table 4. These variables were therefore
290 considered discriminating variables. In this study, CVA was used to find the best linear
291 separation of event type samples using the discriminating variables in Table 4. In order to
292 include only the significantly deviating variables in each catchment CVA, a procedure called
293 forward selection was used. In this procedure, discriminating variables considered on a step-
294 by-step basis and were only included in the model if p values were less than 0.05. This had
295 many advantages because each time a new variable was included in the model, the p values of
296 all non-included variables were updated. The final model included only the variables which
297 were able to discriminate between event types. Each catchment contained a different set of
298 diversifying variables which was able to maximize the difference between event types when
299 viewed in canonical space.

3 Results

3.1 Event type distribution

303 In total 797 storms were identified and analysed for the three catchments between 2000
304 and 2014. Each catchment displayed CW, CCW, figure-of-eight and complex events (Table 5).
305 Hydrological events began under a range of initial base flow conditions. The separating function
306 made clear distinctions between events based on the relation between base flow and quick flow,
307 however, some events could also have been considered sub-events as they were merely peaks
308 which were located on the rising or falling limb of a larger event. CW and CCW (simple event
309 types) contained hysteresis index (HI) values for all ranges of discharge which were either

310 positive (CW) or negative (CCW). Examples of event types are shown in Fig. 3. The CW type
311 event was the most common and CCW events were second in frequency of occurrence. In
312 Oskotz, CW event frequency was three times that of CCW; Latxaga had about twice as many
313 CW events as CCW events; and La Tejería contained nearly the same amount of CW as CCW
314 events. Compound events (complex, figure-of-eight) occurred when a simple event's main peak
315 was preceded by or followed by a secondary (smaller) peak in either discharge or turbidity.
316 Figure-of-eight events consisted of at least one secondary peak in turbidity or discharge that
317 was independent from – or not in sync – with the primary discharge peak. In some cases, the
318 secondary peak was turbidity and came before the main discharge peak. In other cases, the
319 secondary turbidity peak appeared after the main discharge peak. Alternatively, the same event
320 type could have resulted from a storm event having independent, secondary peaks in discharge
321 instead of turbidity. Complex events occurred in two main contexts: first, some resulted from
322 an event having multiple, non-synchronised peaks in both discharge and turbidity. Otherwise
323 they could have occurred due to volatile fluctuations in turbidity during a relatively constant
324 base flow recession periods.

3.2 Seasonal trends in hysteresis index

327 Variation in HI showed slightly different seasonal trends in the different watersheds
328 (Fig. 4). In all three catchments, the average monthly HI (HI_m) gradually decreased from the
329 period November to June. In the more elongated, less-well drained agricultural catchment of
330 Latxaga, a positive HI_m coincided with heavier rains and lower ground cover. The greatest
331 variation in HI for this catchment occurred in September and October and the least variation
332 occurred as the rains became more infrequent (May-June). The Latxaga HI_m drops below zero
333 in March, one month later than in La Tejería. In La Tejería, variation in HI was quite low at the

334 seasonal onset of rains in September and increased through April. Both catchments show
335 steeper declines in HI_m in the period February-April as compared with November-February. In
336 contrast to both agricultural catchments, the forested catchment Oskotz showed most HI
337 variation in February and March. Interestingly, among the three catchments, the HI_m in Oskotz
338 fluctuated the least throughout the year.

340 3.3 Variable controls on event type

341 Canonical variate analysis (CVA) revealed that for each catchment a different
342 combination of discharge, precipitation or vegetation-related variables were most associated
343 with each event type (Fig. 5).

344 For Latxaga, the first canonical axis (a_1) explained 85.5% of the variance between event
345 types and was loaded by the four variables P_{total} , Duration, the turbidity range of the previous
346 storm $T_{range(s-1)}$ and the discharge max of the previous storm $Q_{max(s-1)}$. Based on centroid
347 locations of event groupings, this axis primarily differentiated CW from CCW and figure-of-
348 eight events. CW events tended to receive more rain during the event itself (high P_{total}), were of
349 long Duration and occurred after events with low discharge maximums $Q_{max(s-1)}$ and/or $T_{range(s-1)}$. Analysis of variance (ANOVA; Table 6) confirmed significant differences in group means
350 for Duration ($p=2.93e-3$), $Q_{max(s-1)}$ ($p=2.23e-2$) and $T_{range(s-1)}$ ($p=4.03e-2$). A post-hoc Tukey
351 test confirmed that CW events were longer than CCW in Duration and had lower values for
352 $Q_{max(s-1)}$ ($\alpha=0.01$) and $T_{range(s-1)}$. Lack of adequate sample size for complex events ($n=4$)
353 prevented any meaningful statistical analysis involving complex events. However, it is
354 interesting to note that one complex event which occurred on 2012-10-20 had the highest P_{total}
355 (75.32 mm) of all events in Latxaga. The second canonical axis (a_2) was loaded by rainfall
356 erosivity EI_{30} and T_{max} , though this axis explained only 10% of the variation between storm
357 types. The centroid of the CCW and figure-of-eight events were similar in a_1 but were farther

359 apart in a2, suggesting that events that started off as CCW were likely converted to figure-of-
1
2 360 eight events due to late peaks in turbidity.
3

4
5 361 La Tejería rainfall variables exerted greater control on event type outcome than
6
7 362 discharge variables (Fig. 4b). Q_{mean} , and Q_{max} showed little variation between event types. The
8
9
10 363 first canonical discriminant axis (a1) explained 84.4% of the variance and was most loaded by
11
12 364 30-minute rainfall intensity (I_{30}) and Duration. Just three variables were significantly able to
13
14 365 discriminate between the event types as compared with Latxaga and Oskotz, where four and
15
16
17 366 five variables, respectively, could discriminate between event groupings. Total explained
18
19 367 variance was not affected (Table 5). CCW events were shorter in Duration and occurred under
20
21
22 368 higher rainfall intensities than CW events (Fig. 4b). ANOVA and post hoc Tukey tests
23
24 369 confirmed significant variation between the simple event types in mean I_{30} ($p=1.70e-3$),
25
26
27 370 Duration ($1.92e-05$). Post hoc Tukey test also confirmed figure-of-eight events were
28
29 371 significantly longer than CCW events. Additionally, of the 41 figure-of-eight events from this
30
31
32 372 catchment, 34 began as CW and were later converted to figure-of-eight. API loaded the second
33
34 373 canonical discriminant axis (a2). High I_{30} and high API caused simple CCW events to become
35
36 374 a figure-of-eight. In contrast to the other two catchments, P_{total} did not differ between the simple
37
38
39 375 event types. However, rainfall in the six hours prior to an event (P_{06}) was greater for CCW than
40
41 376 CW events ($2.93E-02$)
42

43
44 377 In Oskotz the first canonical discriminant function (a1) explained 80.8% of the variance
45
46 378 and was most loaded NDVI, P_{total} and T_{LE} . For this reason, a1 is not representative of
47
48
49 379 specifically discharge nor precipitation variables. An ANOVA confirmed that NDVI was
50
51 380 differentiated between all event types ($p= 4.48e-8$) and a post hoc Tukey test indicated that the
52
53 381 only insignificant variation in NDVI existed between CCW and Fig-8 events. P_{total} was greater
54
55
56 382 for CW than CCW events, ($p=1.21e-9$). T_{LE} was significantly longer for CCW than CW events
57
58 383 ($p=6.77e-5$). The second discriminant function (a2) correlated with the I_{60} , EI_{30} and T_{mean} and
59
60
61
62
63
64
65

384 indicated the importance of rainfall intensity and rainfall erosivity in this catchment. An event
385 could have contained just one extra turbidity peak and become a figure-of-eight or could have
386 contained an oscillating turbidity time series and ended up as a complex event. In both cases,
387 high rainfall intensity was present. Figure-of-eight and CCW events tended to occur after more
388 time since the last hydrological event as indicated by the event centroid locations relative to the
389 arrow of T_{LE} . T_{LE} was longer for CCW than CW events ($p=6.77e-5$). ANOVA and post hoc
390 Tukey tests confirmed that event Duration was also longer for CW than for CCW as well as
391 Fig-8 events ($p=6.71e-05$).

393 **3.4 Discharge and differences in magnitude of suspended sediment export**

394 With the exception of the Latxaga catchment, the sign of event HI did not influence the
395 magnitude of turbidity measured at the catchment outlet. Event turbidity mean (T_{mean}) during a
396 runoff event was considered the best available proxy measure of suspended sediment
397 concentration. A two-sample heterogeneous t-test confirmed that T_{mean} from Latxaga was
398 greater for events with a negative HI than for events with a positive HI ($p=0.05$). It has
399 previously been reported that annual sediment concentration is three times higher and annual
400 sediment yield was six times higher in La Tejería than in Latxaga (Casalí et al. 2008). It is thus
401 interesting to note that the T_{mean} in La Tejería for CW events was four times that of Latxaga.
402 However, this was less pronounced for CCW events as T_{mean} in La Tejería was only 2.7 times
403 greater than that of Latxaga. CW events which occurred in winter and spring accounted for
404 most of the suspended sediment which was exported during the study in these two catchments.

405 Channel base flow conditions and the event timing relative to previous events exerted
406 major controls on event type outcome in Latxaga, but this affect was less pronounced in the
407 other two catchments. Graphical analysis of a multi-event hydrograph and turbidity time-series
408 showed that CCW events tended to occur on the recession curve of larger events while CW

409 events tended to occur under very low base flow conditions, or on the rising limb of a larger
410 events (Fig. 6). Results of a one-tailed, heterogeneous variance t-test indicated that positive HI
411 events occurred under lower beginning base flow (Q_b) conditions than events with negative
412 average HI values ($p=0.02$). Q_b showed no significant variation between event type in either La
Tejería or Oskotz.

4 Discussion

4.1 Implications of event classification algorithm

Analysis of the results confirmed that the event categorization algorithm performed well. However, one inconsistency in the algorithm's logic was identified: figure-of-eight events were originally defined as only having one switch in the sign of HI during the event. This meant that some events that are from a manual check are clearly figure eight events should have been categorised as complex. Despite the sign of HI switching twice, the end-of-storm jump in either the discharge or turbidity – the cause of the sign switch – directions did not cause the hysteresis curve to intersect itself. In general, the hysteresis analysis method was highly sensitive to small scale fluctuations in the time-series because the min-max normalisation procedure ensured that the relative shape of the curves remained intact (Lloyd et al. 2015). This allowed the grouping algorithm to capture subtle differences in the time-to-peaks between the curves. This was especially important because the two curves were often in very close proximity. Hysteresis analysis plus event type categorisation in this regard provided extra analytical benefits to hydrological and sedimentological studies (Seeger et al. 2004).

4.2 Explanation of event type distribution

With the exception of very large runoff events, sediment supply in all catchments for CW events was confined to the channel itself, or to the areas directly adjacent to the channel. Complex and

434 figure-of-eight events were exceptions. Heidel (1956) stated that this kind of sediment supply
1
2 435 is characteristic for catchments with small streams, i.e. headwaters or catchments with a dense
3
4 436 drainage pattern. This is in line with the findings of Einstein (1943), stating that suspended
5
6
7 437 sediments and thus suspended sediment peaks normally travel with flow velocity, where
8
9
10 438 maximum discharge peaks travel with the considerably faster wave velocity. The difference
11
12 439 between both is less pronounced in smaller catchments due to the shorter travel distances,
13
14 440 resulting in smaller differences in response time. The dominant presence of CW hysteresis in
15
16 441 Latxaga and Oskotz is likely explained by the increased catchment morphological complexity
17
18 442 and vegetative features of these two catchments. The steeper average channel gradients of La
19
20 443 Tejería, in combination with a lower stream density and lack of channel vegetation leads to a
21
22 444 more erosive flow. Or, the more erosive flow in La Tejería created steeper channel gradients
23
24 445 and a lack of channel vegetation and subsequent high occurrence of bank failures, especially in
25
26 446 the latest stages of the rainfall event, also supports the highest importance of counter-clockwise
27
28 447 loops in La Tejería (Figure 7). Subsequently, suspended sediment in La Tejería had little change
29
30
31 448 for in-stream deposition because of the too high flow velocities in relation with the grain size
32
33
34 449 distribution of the sediments. This is in line with the fact that La Tejería shows much higher
35
36 450 sediment yields, compared to Latxaga, so in-stream sediment storage seems to play a crucial
37
38 451 role. In addition, the morphological and topographic differences between watersheds, La
39
40 452 Tejería shows a more circular shaped (see shape factor and Gravelius Index, Table 1), with a
41
42 453 smoother topography and a higher general slope gradient of the stream channels than those of
43
44 454 the Latxaga watershed. The circular shape (illustrated also by the shape factor (K_f , Table 1)),
45
46 455 flatter topography and higher average slope gradient of stream channels causes more efficient
47
48 456 runoff generation which higher peak discharges at the outlet. Moreover, the more complex
49
50
51 457 topography, with a floodplain and more abundant riparian vegetation in Latxaga, favour
52
53 458 sedimentation within the catchment before reaching the outlet. The effect of the catchment
54
55
56
57
58
59
60
61
62
63
64
65

459 complexity on the amount of sediment yield was also shown by a modelling effort by Casali et
1
2 460 al. (2008) who found that Latxaga's elongated shape reduced the sediment yield three to five
3
4
5 461 times compared to the rounded La Tejeria catchment.
6

7 462
8 463 The figure-of-eight and complex hysteresis events indicate the initiation of sediment
9
10 464 connectivity between the sampling location and remote sources of sediment, i.e. non-channel
11
12
13 465 of up-catchment sources. In both Latxaga and La Tejería, figure-of-eight hysteresis events that
14
15
16 466 started as CW events tended to occur under low-flow conditions, whereas figure-of-eight
17
18 467 hysteresis events that started as CCW tended to occur under higher flow conditions. In La
19
20
21 468 Tejería has steeper average channel gradients and lack of channel vegetation. Therefore, the
22
23 469 erosion processes can be explained by late-stage river bank collapses, as well as a combination
24
25 470 of saturation excess and infiltration excess overland flow, which contains freshly mobilised
26
27
28 471 sediment due to high rainfall intensities. In this La Tejería catchment, oscillations in turbidity
29
30 472 during the discharge recession implicate up-catchment sediment connectivity or slow
31
32
33 473 responding in-stream sediment additions. Once the hillslope sediments reached the outlet, the
34
35 474 turbidity increased while the channel discharge already was in the after-peak recession. Seeger
36
37
38 475 et al. (2004) showed that when the rainfall intensity decreases, the generation of Hortonian
39
40 476 overland flow will subside. In La Tejería however, the decline in the suspended sediment
41
42 477 concentration was faster than the decline in discharge. As a result, without a high API, CCW
43
44
45 478 events in La Tejería tended to remain CCW rather than converting to figure-of-eight or complex
46
47 479 events.
48

49
50 480

51 52 481 **4.3 Hysteresis analysis as a signal of sediment and hydrological connectivity** 53

54 482 Hysteresis loops capture the discrepancy between discharge and suspended sediment
55
56
57 483 concentration during runoff events (Gao and Josefson 2012). This analysis of three small
58
59
60 484 catchments in Northwest Spain revealed patterns which could link discharge and suspended
61

485 sediment concentrations as products of non-linearity in hydrological connections via overland
1
2 486 flow (runoff) and associated sediment connections due to sediment entrainment (Bracken et al.
3
4 487 2015; Keesstra et al., 2018). It was found that spatial and temporal variability of erosion,
5
6 488 transport and sedimentation were continuously changing due to variation in catchment and
7
8 489 channel state before and during a storm event, which is in line with similar findings by Cooper
9
10 et al. (2007). The variation in transport times between water to channel outlet were explained
11
12 490 by variations in hydrological and sediment connectivity (Bracken and Croke 2007; Bracken et
13
14 491 al. 2015; Parsons et al. 2015; Poepl et al. 2017). These types of connectivity could be linked
15
16 492 to complex landscape and channel morphology and could also be linked to the feedback
17
18 493 mechanisms between sediment source locations, transport pathways and sinks (Heckmann and
19
20 494 Vericat 2018), such as the co-evolution of riparian vegetation and floodplain sedimentation.
21
22 495 The forested Oskotz catchment showed decreased sediment connectivity between hillslopes and
23
24 496 the channel. However, because of tree cutting, bare land patches were formed. These act as
25
26 497 sediment sources from which overland flow at intense rain storms can develop. This overland
27
28 498 flow brings sediments to the channel (Casalí et al. 2010). Finally, La Tejería with its steeper
29
30 499 gradients, deeper channel incision and non-vegetated channel bed (Fig. 7), displayed much
31
32 500 more surface hydrological (runoff) as well as sediment connectivity. The overall sediment yield
33
34 501 was three to five times higher (Casali et al., 2010) and this catchment displayed a more balanced
35
36 502 HI distribution between CW and CCW events.
37
38
39
40
41
42
43
44
45

46 504 Therefore, we conclude that a hysteresis analysis can be a good method for assessing
47
48 505 sediment connectivity on small catchment scale. Because we have good knowledge of the
49
50 506 catchment dynamics in these systems, from other studies conducted in these catchments (Casali
51
52 507 et al., 2008, 2010, 2012; Masselink et al., 2016, 2017) it is possible to link the catchment
53
54 508 complexity to a majority of CW loops; and high sediment yields and low complexity to a more
55
56 509 mixed CCW and CW system. Even though this study did not include an explicit analysis of the
57
58
59
60
61
62
63
64
65

1 hillslope erosion processes, it was possible to capture the emergent nature of the sediment
2 transport through continuous and systematic classification of differences in water and sediment
3 delivery at the catchment outlet. The extensive use of data on the initial hydrological state of a
4 catchment agrees with Faulkner's (2008) definition of sediment connectivity, which states that
5 sediment connectivity incorporates the integrated status of a system within the catchment.
6
7
8
9
10

11 515

12 516 **5 Conclusions**

13
14
15
16
17
18 517 The use of hysteresis analysis on 10 minute hydrological and turbidity data in this study
19 allowed for a detailed analysis of sediment and fine-grained sediment transport to streams
20 located in three contrasting morphological, hydrogeological and landscape character
21 catchments under event flow conditions. The quantitative method developed in this paper
22 includes all available data, and allowed for the first time, rain storms to be automatically
23 classified based on a range of HI distributions throughout the event for all events in the rainfall
24 record of in this case up to ##years. The data on catchments initial state and previous
25 precipitation events has also proven to provide useful data with which the connectivity analysis
26 could be compared and validated.
27
28
29
30
31
32
33
34
35
36
37
38
39
40

41 526 In the Spanish catchments where the tool was tested clockwise hysteresis was more dominant
42 in the more disconnected catchments of Latxaga and Oskotz. Counter-clockwise hysteresis
43 occurred equally as much as clockwise hysteresis in La Tejería, with its circular shape and
44 relatively deeply incised channel. Complex event types (figure-of-eight; complex) in all
45 catchments were the result of runoff and sediment connectivity between the channel and
46 hillslopes.
47
48
49
50
51
52
53
54

55
56
57 532 Hysteresis analysis is a valuable tool for assessing event sediment transport behaviours and
58 provided a robust method for comparing how catchments function to generate and transport
59
60
61
62

1
2
3
4
5
6
7
8
9
10
11
12
13
14
15
16
17
18
19
20
21
22
23
24
25
26
27
28
29
30
31
32
33
34
35
36
37
38
39
40
41
42
43
44
45
46
47
48
49
50
51
52
53
54
55
56
57
58
59
60
61
62
63
64
65

534 sediment as well as to assess the state of sediment connectivity. It has further shown that these
535 differences sediment transport times result emerge over time differently due to catchment
536 morphological complexity, distribution and intensity of vegetation and topographical factors.
537 Knowledge from this type of analysis can lead to further application of the algorithm herein
538 described, in order to identify sediment source locations, transport pathways and sink locations.
539 It can therefore be of use to catchment managers who are seeking robust, cost effective and
540 precise ways to mitigate excess sediment losses on and between fields. Including all available
541 data in terms of water and sediment discharge makes the technique more reliable than most
542 other studies using hysteresis, where an only a selection of the storms is evaluated.

543
Acknowledgements This study was supported by the effective network that was created in
COST Action CONNECTEUR (ES1306, Connecting European Connectivity Research).
Furthermore, we would like to acknowledge the support of the Research Project CGL2015-
64284-C2-1-R, founded by the Spanish Ministry of Economy and Competitiveness.

549 **References**

- 550 Aich V, Liersch S, Vetter T, Huang S, Tecklenburg J, Hoffmann P, Koch H, Fournet S,
551 Krysanova V, Müller E, Hattermann FF (2014) Comparing impacts of climate change on
552 streamflow in four large African river basins. *Hydrol Earth Syst Sci* 4:1305
- 553 Bilotta GS, Brazier, R E (2008) Understanding the influence of suspended solids on water
554 quality and aquatic biota. *Water Res* 42:2849-2861

- 1
2
3
4
5
6
7
8
9
10
11
12
13
14
15
16
17
18
19
20
21
22
23
24
25
26
27
28
29
30
31
32
33
34
35
36
37
38
39
40
41
42
43
44
45
46
47
48
49
50
51
52
53
54
55
56
57
58
59
60
61
62
63
64
65
- 555 Bird G, Brewer PA, Macklin MG, Nikolova M, Kotsev T, Mollov M, Swain C (2010)
556 Quantifying sediment-associated metal dispersal using Pb isotopes: Application of binary
557 and multivariate mixing models at the catchment-scale. *Environ Pollut* 158(6):2158-2169
- 558 Bracken LJ, Croke J (2007). The concept of hydrological connectivity and its contribution to
559 understanding runoff-dominated geomorphic systems. *Hydrol Process* 21:1749–1763.
- 560 Bracken LJ, Turnbull L, Wainwright J, Bogaart P (2015) Sediment connectivity: A framework
561 for understanding sediment transfer at multiple scales. *Earth Surf Process Landforms*
562 40:177–188. doi: 10.1002/esp.3635
- 563 Brown LC, Foster GR (1987) Storm erosivity using idealized intensity distributions. *Trans*
564 *ASAE* 30:379-386
- 565 Casalí J, Gastesi R, Álvarez-Mozos J, De Santisteban LM, de Lersundi JDV, Giménez R, ...
566 López JJ (2008). Runoff, erosion, and water quality of agricultural watersheds in central
567 Navarre (Spain). *Agr Water Manage* 95:1111-1128
- 568 Casalí J, Giménez R, Díez J, Álvarez-Mozos J, de Lersundi JDV, Goñi, M, López J (2010)
569 Sediment production and water quality of watersheds with contrasting land use in Navarre
570 (Spain). *Agr Water Manage* 97:1683-1694
- 571 Casalí J, Loizu J, Campo MA, De Santisteban LM, Álvarez-Mozos (2012) Runoff, erosion and
572 water quality of agricultural watersheds in central Navarre (Spain). *Agr Water Manage*
573 110: 1-8
- 574 Cerdà A, Keesstra SD, Rodrigo-Comino J, Novara A, Pereira P, Brevik E, Giménez-Morera A,
575 Fernández-Raga M, Pulido M, di Prima S, Jordán A (2017) Runoff initiation, soil

576 detachment and connectivity are enhanced as a consequence of vineyards plantations. J
1
2 577 Environ Manage 202:268–275. <https://doi.org/10.1016/j.jenvman.2017.07.036>
3
4
5
6 578 Cerro C, Bech J, Codina B, Lorente J (1998) Modeling rain erosivity using disdrometric
7
8 579 techniques. Soil Sci Soc Am J 62:731–735
9
10
11
12 580 Cooper JR, Wainwright J, Parsons AJ, Onda Y, Fukuwara T, Obana, E, Hargrave, GH (2012).
13
14 581 A new approach for simulating the redistribution of soil particles by water erosion: A
15
16 582 marker- in- cell model. J Geophys Res: Earth Surface 117(F4)
17
18
19
20 583 Dash J, Mathur A, Foody GM, et al (2007) Land cover classification using multi-temporal
21
22 584 MERIS vegetation indices. Int J Remote Sens 28:1137–1159. doi:
23
24 585 10.1080/01431160600784259
25
26
27
28
29 586 Eckhardt K (2005). How to construct recursive digital filters for baseflow separation. Hydrol
30
31 587 Process 19:507-515
32
33
34
35 588 Einstein HA (1943) Flow on a movable bed. Proc Hydraulic Conf Univ of Iowa Bulletin, pp
36
37 589 333–341
38
39
40
41 590 Faulkner H (2008) Connectivity as a crucial determinant of badland morphology and evolution.
42
43 591 Geomorphology 100:91-103
44
45
46
47 592 Gao P, Josefson M (2012) temporal variations of suspended sediment transport in Oneida Creek
48
49 593 watershed, central New York. J Hydrol 426-427:17–27
50
51
52
53 594 Gao P, Pasternack G (2007) Dynamics of suspended sediment transport at field- scale drain
54
55 595 channels of irrigation- dominated watersheds in the Sonoran Desert, southeastern
56
57 596 California. Hydrol Process 21:2081-2092
58
59
60
61
62
63
64
65

- 597 García-Ruiz JM, Nadal-Romero E, Lana-Renault N, Beguería S (2013) Erosion in
1
2 598 Mediterranean landscapes: Changes and future challenges. *Geomorphology* 198:20–36
3
4
5
6 599 Gentile F, Bisantino T, Corbino R, Milillo F, Romano G, Liuzzi GT (2010) Monitoring and
7
8 600 analysis of suspended sediment transport dynamics in the Carapelle torrent (southern
9
10 601 Italy). *Catena* 80:1-8
11
12
13
14 602 Heckmann T, Vericat D (2018) Computing spatially distributed sediment delivery ratios:
15
16 603 Inferring functional sediment connectivity from repeat high-resolution digital elevation
17
18 604 models. *Earth Surf Process Landforms*. doi: 10.1002/esp.4334
19
20
21
22
23 605 Heidel SG (1956) The progressive lag of sediment concentration with flood waves. *EOS*
24
25 606 37:56–66
26
27
28
29 607 Jansson MB (2002) Determining sediment source areas in a tropical river basin, Costa Rica.
30
31 608 *Catena* 47:63-84
32
33
34
35 609 Keesstra SD, van Dam O, Verstraeten G, van Huissteden J, (2009) Changing sediment
36
37 610 dynamics due to natural reforestation in the Dragonja catchment, SW Slovenia. *Catena*
38
39 611 78:60–71. <https://doi.org/10.1016/j.catena.2009.02.021>
40
41
42
43 612 Keesstra S, Nunes JP, Saco P, Parsons T, Poepl R, Masselink R, Cerdà A, (2018) The way
44
45 613 forward: Can connectivity be useful to design better measuring and modelling schemes for
46
47 614 water and sediment dynamics? *Sci. Total Environ.* 644.
48
49 615 <https://doi.org/10.1016/j.scitotenv.2018.06.342>
50
51
52
53
54 616 Kjelland ME, Woodley CM, Swannack TM, Smith DL (2015) A review of the potential effects
55
56 617 of suspended sediment on fishes: potential dredging-related physiological, behavioral, and
57
58 618 transgenerational implications. *Environment Systems and Decisions* 35:334–350
59
60
61
62
63
64
65

- 619 Klein M (1984) Anti clockwise hysteresis in suspended sediment concentration during
1
2 individual storms: Holbeck Catchment; Yorkshire, England. *Catena* 11:251-257
3
4
5
6 621 Langlois JL, Johnson DW, Mehuys GR (2005) Suspended sediment dynamics associated with
7
8 snowmelt runoff in a small mountain stream of Lake Tahoe (Nevada). *Hydrol Process*
9
10 623 19:3569-3580
11
12
13
14 624 Lawler DM, Petts GE, Foster ID, Harper S (2006) Turbidity dynamics during spring storm
15
16 events in an urban headwater river system: The Upper Tame, West Midlands, UK. *Sci*
17 625
18
19 626 *Total Environ* 360:109-126
20
21
22
23 627 Linsley RK, Kohler MA (1951) Variations in storm rainfall over small areas. *Eos, Transactions*
24
25 628 *American Geophysical Union* 32: 245-250
26
27
28
29 629 Lloyd CEM, Freer JE, Johnes PJ, Collins AL (2016) Using hysteresis analysis of high resolution
30
31 water quality monitoring data, including uncertainty, to infer controls on nutrient and
32 630
33 sediment transfer in catchments. *Sci Total Environ* 543:388–404
34 631
35
36
37
38 632 López-Tarazón JA, Batalla RJ, Vericat D, Francke T (2009). Suspended sediment transport in
39
40 a highly erodible catchment: the River Isábena (Southern Pyrenees). *Geomorphology*
41
42 634 109:210-221
43
44
45
46 635 Mano V, Nemery J, Belleudy P, Poirel A (2009) Assessment of suspended sediment transport
47
48 in four alpine watersheds (France): influence of the climatic regime. *Hydrol Process* 5:777-
49 636
50 792
51 637
52
53
54
55 638 Masselink RJH, Keesstra SD, Temme AJAM, Seeger M, Giménez R, Casalí J (2016) Modelling
56
57 discharge and sediment yield at catchment scale using connectivity components. *Land*
58 639
59
60 640 *Degrad Dev* 27:933–945
61
62

- 641 Masselink RJH, Temme AJAM, Giménez R, Casalí J, Keesstra SD (2017) Assessing hillslope-
1
2 642 channel connectivity in an agricultural catchment using rare-earth oxide tracers and
3
4 643 random forests models | Valorando la conectividad ladere-cauce en una cuenca agrícola,
5
6
7 644 utilizando óxidos de tierras raras como trazadores y modelos de. Cuad. Investig. Geogr.
8
9 645 43, 19–39. <https://doi.org/10.18172/cig.3169>
10
11
12
13 646 Morgan RPC (2005) Soil erosion and conservation. Longman Group Limited, UK, pp 63–74
14
15
16
17 647 Nathan R J, McMahon TA (1990) Evaluation of automated techniques for base flow and
18
19 648 recession analyses. *Water Resour Res* 26:1465-1473
20
21
22
23 649 Owens PN, Walling DE (2002) The phosphorus content of fluvial sediment in rural and
24
25 650 industrialized river basins. *Water Res* 36:685-701
26
27
28
29 651 Parsons AJ, Wainwright J, Brazier RE, Powell DM (2006) Is sediment delivery a fallacy? *Earth*
30
31 652 *Surface Processes Landforms* 31:1325–1328
32
33
34
35 653 Parsons AJ, Bracken L, Poepl RE et al (2015) Introduction to special issue on connectivity in
36
37 654 water and sediment dynamics. *Earth Surf Process Landforms* 40:1275–1277. doi:
38
39 655 10.1002/esp.3714
40
41
42
43 656 Poepl RE, Keesstra SD, Maroulis J (2017) A conceptual connectivity framework for
44
45 657 understanding geomorphic change in human-impacted fluvial systems. *Geomorphology*
46
47 658 277:237–250. doi: 10.1016/j.geomorph.2016.07.033
48
49
50
51
52 659 Regüés D, Guàrdia R, Gallart, F (2000). Geomorphic agents versus vegetation spreading as
53
54 660 causes of badland occurrence in a Mediterranean subhumid mountainous area. *Catena*
55
56 661 40:173–187
57
58
59
60
61
62

- 1
2
3
4
5
6 662 Roehl JE (1962) Sediment source areas, delivery ratios and influencing morphological factors.
7
8
9 663 Int Assoc Hydrol Sci Publ 59:202–213
10
11
12 664 Rovira A, Batalla RJ (2006) Temporal distribution of suspended sediment transport in a
13
14 665 Mediterranean basin: The Lower Tordera (NE SPAIN). *Geomorphology* 79:58-71
15
16
17 666 Seeger M, Errea MP, Begueria S, Arnáez J, Marti C, García-Ruiz JM (2004). Catchment soil
18
19 667 moisture and rainfall characteristics as determinant factors for discharge/suspended
20
21 668 sediment hysteretic loops in an small headwater catchment in the Spanish Pyrenees. *J*
22
23 669 *Hydrol* 288:299–311
24
25
26 670 Sherriff SC, Rowan JS, Melland AR, Jordan P, Fenton O, Huallachain DO (2015) Investigating
27
28 671 suspended sediment dynamics in contrasting agricultural catchments using ex situ
29
30 672 turbidity-based suspended sediment monitoring. *Hydrol Earth Syst Sci* 19:3349–3363
31
32
33 673 Sith R, Yamamoto T, Watanabe A, Nakamura T, Nadaoka K (2017) Analysis of Red Soil
34
35 674 Sediment Yield in a Small Agricultural Watershed in Ishigaki Island, Japan, Using Long–
36
37 675 Term and High Resolution Monitoring Data. *Environ Process*, pp 1-22
38
39
40 676 Sloto RA, Crouse MY (1996) HYSEP, a computer program for streamflow hydrograph
41
42 677 separation and analysis. US Department of the Interior, US Geological Survey
43
44
45
46 678 Smith HG, Dragovich D (2009) Interpreting sediment delivery processes using suspended
47
48 679 sediment-discharge hysteresis patterns from nested upland catchments, south-eastern
49
50 680 Australia. *Hydrol Process* 23:2415
51
52
53
54 681 Song Y, Ji J, Yang Z, Yuan X, Mao C, Frost RL, Ayoko GA (2011) Geochemical behavior
55
56 682 assessment and apportionment of heavy metal contaminants in the bottom sediments of
57
58 683 lower reach of Changjiang River. *Catena* 85:73-81
59
60
61
62
63
64
65

- 1
2
3
4
5
6
7
8
9
10
11
12
13
14
15
16
17
18
19
20
21
22
23
24
25
26
27
28
29
30
31
32
33
34
35
36
37
38
39
40
41
42
43
44
45
46
47
48
49
50
51
52
53
54
55
56
57
58
59
60
61
62
63
64
65
- 684 Stubblefield AP, Reuter JE, Dahlgren RA, Goldman CR (2007) Use of turbidometry to
685 characterize suspended sediment and phosphorus fluxes in the Lake Tahoe basin,
686 California, USA. *Hydrol Process* 21:281-291
- 687 Ter Braak CJF, Smilauer P (2012) *CANOCO 5*. Biometris, Wageningen, The Netherlands
- 688 Wainwright J, Turnbull L, Ibrahim TG, Lexartza-Artza I, Thornton SF, Brazier RE (2011)
689 Linking environmental regimes, space and time: Interpretations of structural and
690 functional connectivity. *Geomorphology* 126:387–404
- 691 Wotling G, Bouvier CH (2002) Impact of urbanization on suspended sediment and organic
692 matter fluxes from small catchments in Tahiti. *Hydrol Process* 16:1745-1756
- 693 Zabaleta A, Martínez M, Uriarte JA, Antigüedad I (2007) Factors controlling suspended
694 sediment yield during runoff events in small headwater catchments of the Basque Country.
695 *Catena* 71:179-190
- 696 Zhou H, Chang W, Zhang L (2016) Sediment sources in a small agricultural catchment: A
697 composite fingerprinting approach based on the selection of potential sources.
698 *Geomorphology* 266:11-19
- 699 Ziegler AD, Benner SG, Tantasirin C, Wood SH, Sutherland RA, Sidle RC, Jachowski N,
700 Nullet M, Xi LX, Snidvongs A, Giambelluca TW, Fox JF (2014) Turbidity-based sediment
701 monitoring in northern Thailand: Hysteresis, variability, And uncertainty. *J Hydrol*
702 *519:2020–2039*

703 **List of figures:**

704 **Fig. 1.** Study area: Latxaga, La Tejería and Oskotz watersheds are part of the experimental
705 agricultural watershed network of the Government of Navarre.

706 **Fig. 2** (a) Example (model) storm of a clockwise hysteresis where turbidity peaks before
707 discharge and (b) model of a counter-clockwise hysteresis event where turbidity peaks after
708 discharge

709 **Fig. 3** Plots showing temporal hydrograph and turbidity graphs as well as hysteresis plots (a)
710 CW - Latxaga; (b) CCW - Latxaga; (c) CW-Eight - La Tejería; (d) CCW-Eight - Oskotz; (e)
711 CCW-Complex-Oskotz; (f) CW-Complex - Oskotz. The vertical dashed lines mark the start
712 and stop times for each event

713 **Fig. 4** Average monthly HI values plus monthly HI standard deviation

714 **Fig. 5** Chart results of canonical variate analysis (a) Latxaga; (b) La Tejería; and (c) Oskotz

716 **List of tables:**

717 **Table 1.** Catchment environmental characteristics

718 **Table 2.** Base flow separation model filter constants by catchments

719 **Table 3.** Event type separation procedure based on sign of HI value calculated for each
720 discharge quartile

721 **Table 4.** Runoff event variables and descriptions

722 **Table 5:** Total recorded event type for each catchment

723 **Table 6:** Results of the canonical variate analysis

725 **Table 7.** Results of ANOVA showing differences in mean values of event storm variables

Table 1. Catchment environmental characteristics

	Latxaga	Tejeria	Oskotz
Location	42°47'7.5"N 1°26'11.4"W	42°44'710.6"N 1°56'57.2"W	42°57'29.14"N 1°46'43.58"W
Area (km²)	2.07	1.69	5.05
Perimeter (km)	6.67	5.46	11.44
Total channel length (km)	5.38	3.2	7.41
Minimum elevation (m)	504	496	539
Maximum elevation (m)	639	649	792
Av slope (%)	19.3	14.8	19.8
Av. (permanent) channel slope (%)	12.4	14.6	5.1
Climate	Humid submediterranean	Humid submediterranean	Sub-Atlantic
Annual precipitation (mm)	835	725	1242
Rainfall days	100	105	130
Av. Temperature °C	12	13	12
Lithology	Marls, grey marls	Marls, sandstones	Marls
Gravelius index	1.30	1.17	0.92
Shape Factor	0.26	0.54	0.37
Drainage density (km km²)	2.61	1.91	1.94

Table 2. Base flow separation model filter constants by catchments

Catchment	a	BFI _{max}	Flow regime	Aquifer Porosity
Latxaga	0.963	0.50	ephemeral	porous
La Tejería	0.963	0.50	ephemeral	porous
Oskotz	0.963	0.50	ephemeral	porous

Table 3. Event type separation procedure based on sign of HI value calculated for each discharge quartile

Event Type Code	Grouping ₁	Grouping ₂	HI _{q1}	HI _{q2}	HI _{q3}	HI _{q4}
1	CW	CW	+	+	+	+
2	CW	CW	+	+	+	-
3	CW	Figure-of-eight	+	+	-	-
4	CW	Figure-of-eight	+	+	-	+
5	CCW	CCW	+	-	-	-
6	CW	Figure-of-eight	+	-	-	+
7	CW	Complex	+	-	+	+
8	CW	Complex	+	-	+	-
9	CCW	CCW	-	-	-	-
10	CCW	CCW	-	-	-	+
11	CCW	Figure-of-eight	-	-	+	+
12	CCW	Figure-of-eight	-	-	+	-
13	CW	CW	-	+	+	+
14	CCW	Figure-of-eight	-	+	+	-
15	CCW	Complex	-	+	-	+
16	CCW	Complex	-	+	-	-

Table 4. Runoff event variables and descriptions

Runoff event parameters	
Rainfall variables	Event discharge and turbidity variables
Total precipitation, P_{total} (mm)	Time elapsed since last runoff event, T_{LE} (hours)
Event duration, Duration (hours)	Baseflow at the start of event, Q_b (L s ⁻¹)
Antecedent precipitation index 7 days before event, API (mm)	Mean stream discharge, Q_{mean} (L s ⁻¹)

Maximum averaged 30 minute rainfall, P_{30max} (mm)
 Maximum averaged 60 minute rainfall, P_{60max} (mm)
 Maximum averaged 120 minute rainfall, P_{120max} (mm)
 30 minute rainfall intensity, I_{30} (mm)
 60 minute rainfall intensity, I_{60} (mm)
 Rainfall erosivity, EI_{30} ($MJ\ mm^{-1}\ ha^{-1}\ h^{-1}$)

Turbidity/Suspended sediment variables

Average turbidity, T_{mean} (NTU)
 Maximum turbidity, T_{max} (NTU)
 Minimum turbidity, T_{min} (NTU)
 Range of turbidity, T_{range} (NTU)
 Maximum turbidity previous storm, $T_{max(s-1)}$ (NTU)
 Minimum turbidity, $T_{min(s-1)}$ (NTU)
 Range of turbidity previous storm, $T_{range(s-1)}$ (NTU)

Maximum/peak stream discharge Q_{max} ($L\ s^{-1}$)
 Minimum stream discharge Q_{min} ($L\ s^{-1}$)
 Range of stream discharge Q_{range} ($L\ s^{-1}$)
 Maximum stream discharge from previous storm, $Q_{max(s-1)}$ ($L\ s^{-1}$)
 Minimum stream discharge from previous storm, $Q_{min(s-1)}$ ($L\ s^{-1}$)
 Range of stream discharge previous storm $Q_{range(s-1)}$ ($L\ s^{-1}$)

Other variables

Normalized difference vegetation index, **NDVI** (--)

Table 5: Total recorded event type for each catchment

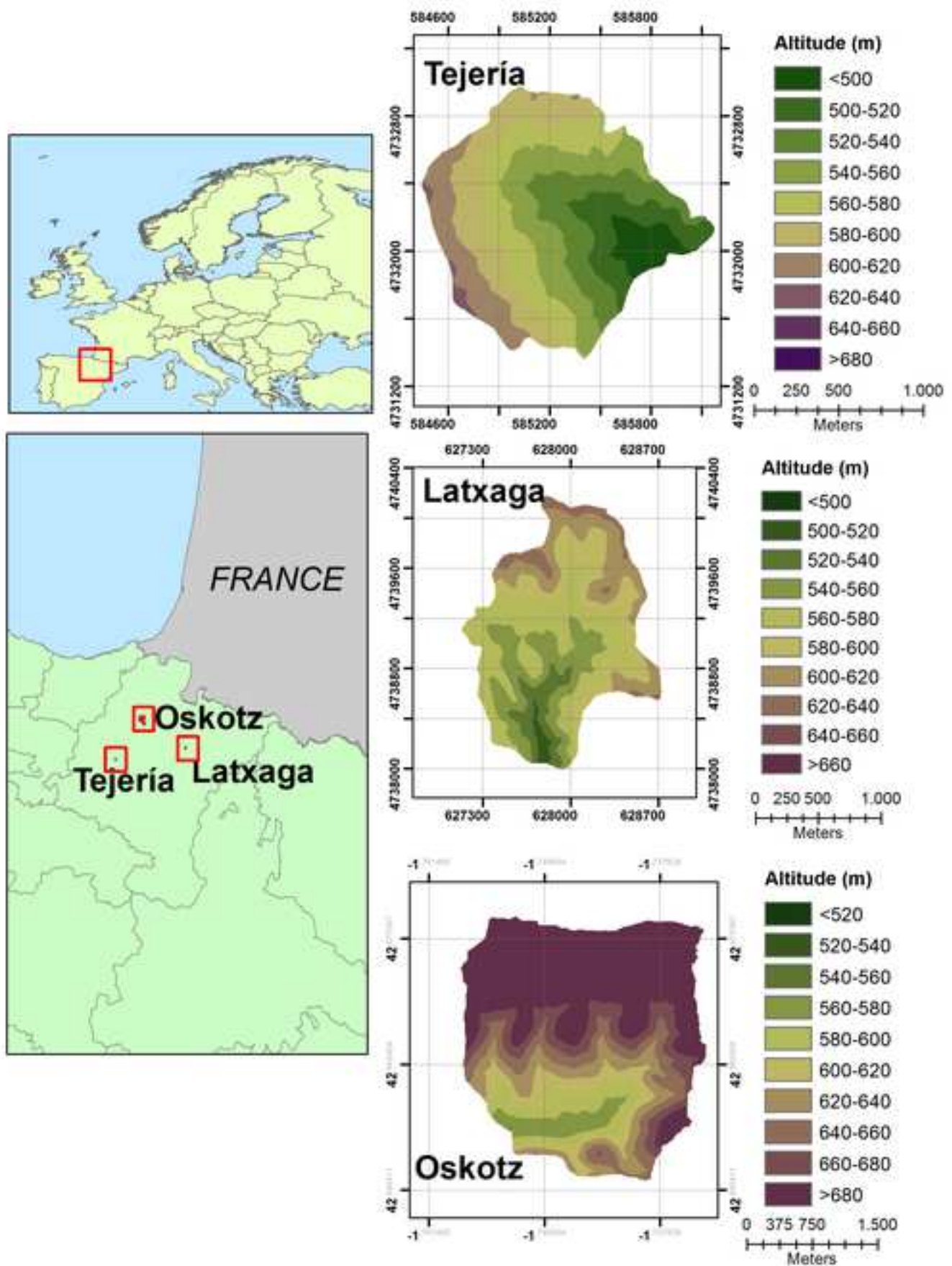
Catchment	CW	CCW	Fig8	Complex	Total
Latxaga	137	60	17	4	218
OskotzF	242	74	44	13	373
Tejeria	81	80	32	13	206
Total	460	214	90	35	797

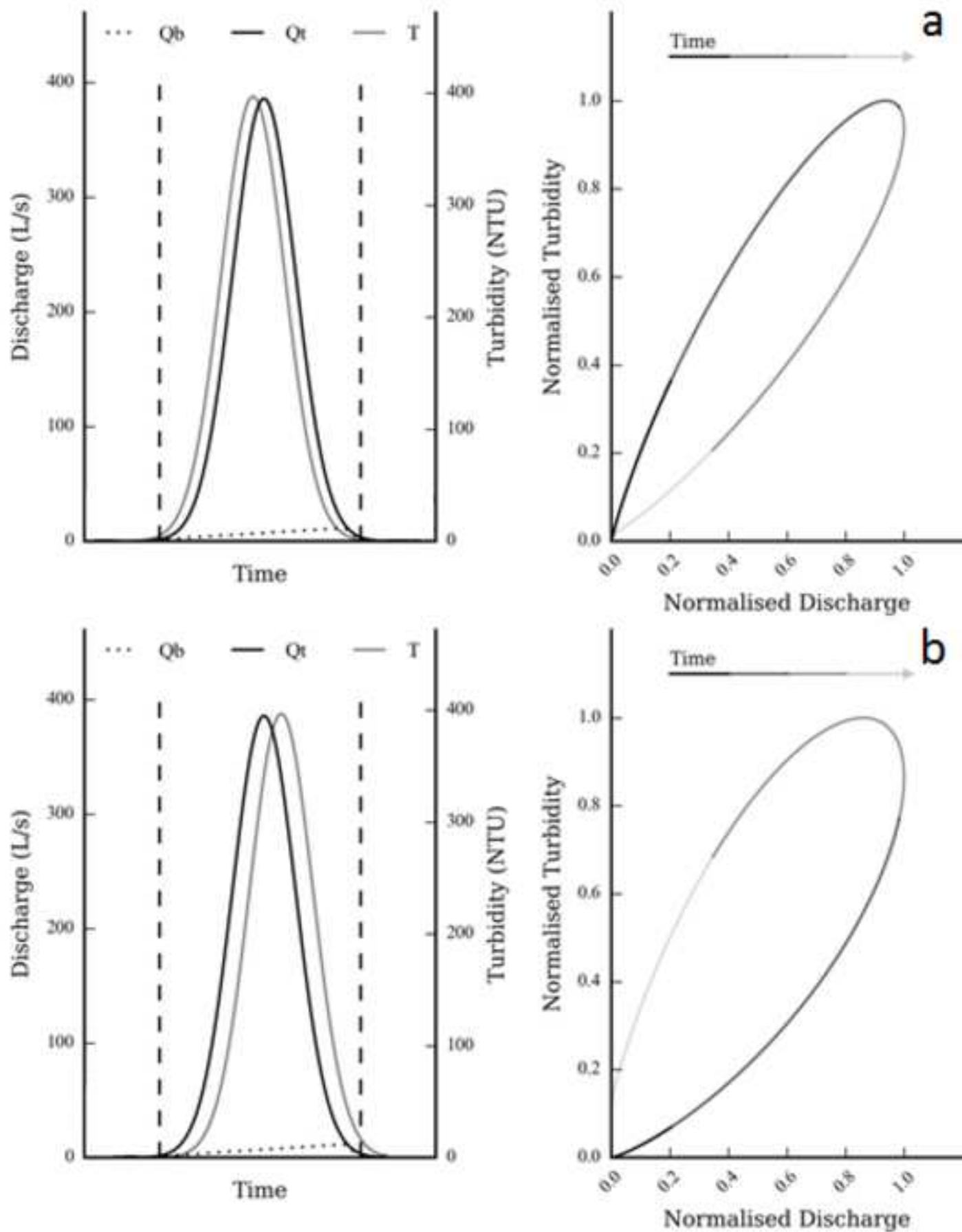
Table 6: Results of the canonical variate analysis

Canonical Variate Analysis: Latxaga				Canonical Variate Analysis: Tejeria				Canonical Variate Analysis: Oskotz						
Discriminant axes summary:				Discriminant axes summary:				Discriminant axes summary:						
Statistic	Ax 1	Ax 2		Statistic	Ax 1	Ax 2		Statistic	Ax 1	Ax 2				
Eigenvalue	0.46	0.05		Eigenvalue	0.25	0.07		Eigenvalue	0.36	0.03				
Percent variance	85.5%	95.0%		Percent variance	84.4%	99.0%		Percent variance	90.6	98.5				

Table 7. Results of ANOVA showing differences in mean values of event storm variables

Catchment	Latxaga					La Tejeria					Oskotz				
	CW	CCW	Fig8	Complex	p	CW	CCW	Fig8	Complex	p	CW	CCW	Fig8	Complex	p
Ptotal	16.74	10.18	8.14	24.20	2.90E-03	14.51	12.63	13.91	18.73	-	23.48	10.22	14.98	9.25	1.21E-09
Duration	36.09	23.62	26.33	35.38	3.14E-05	24.95	15.96	22.93	28.50	3.95E-06	46.83	32.31	34.38	41.17	6.72E-05
P ₀₆						2.59	4.58	3.20	3.09	2.93E-02					
I30						3.84	6.81	3.20	2.61	1.67E-03					
Q _{max(s-1)}	150.45	223.42	179.13	138.68	2.95E-02										
T _{range(s-1)}	469.92	832.48	483.73	151.54	4.20E-03										
NDVI											166.46	179.23	217.88	270.85	4.49E-08





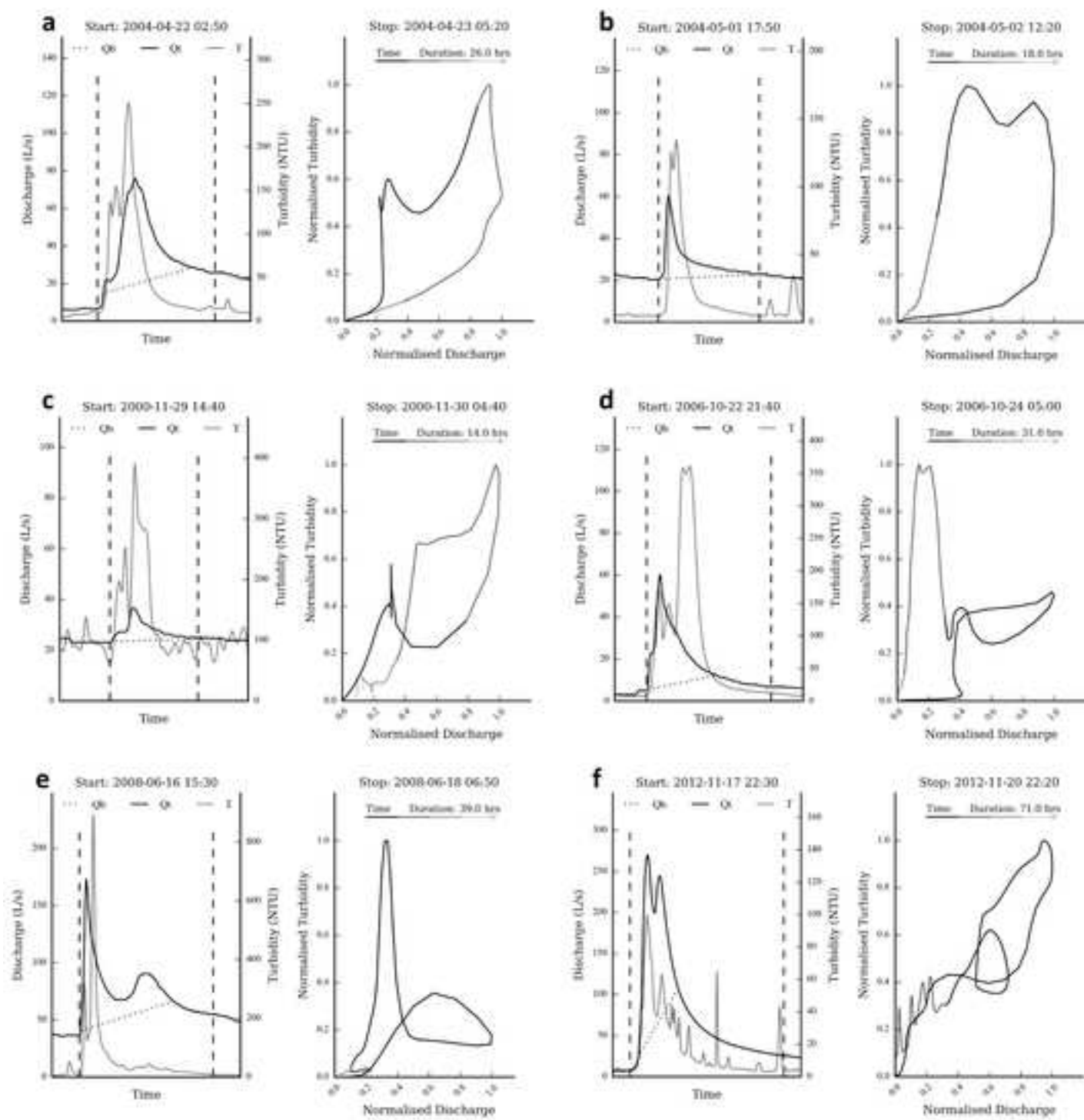
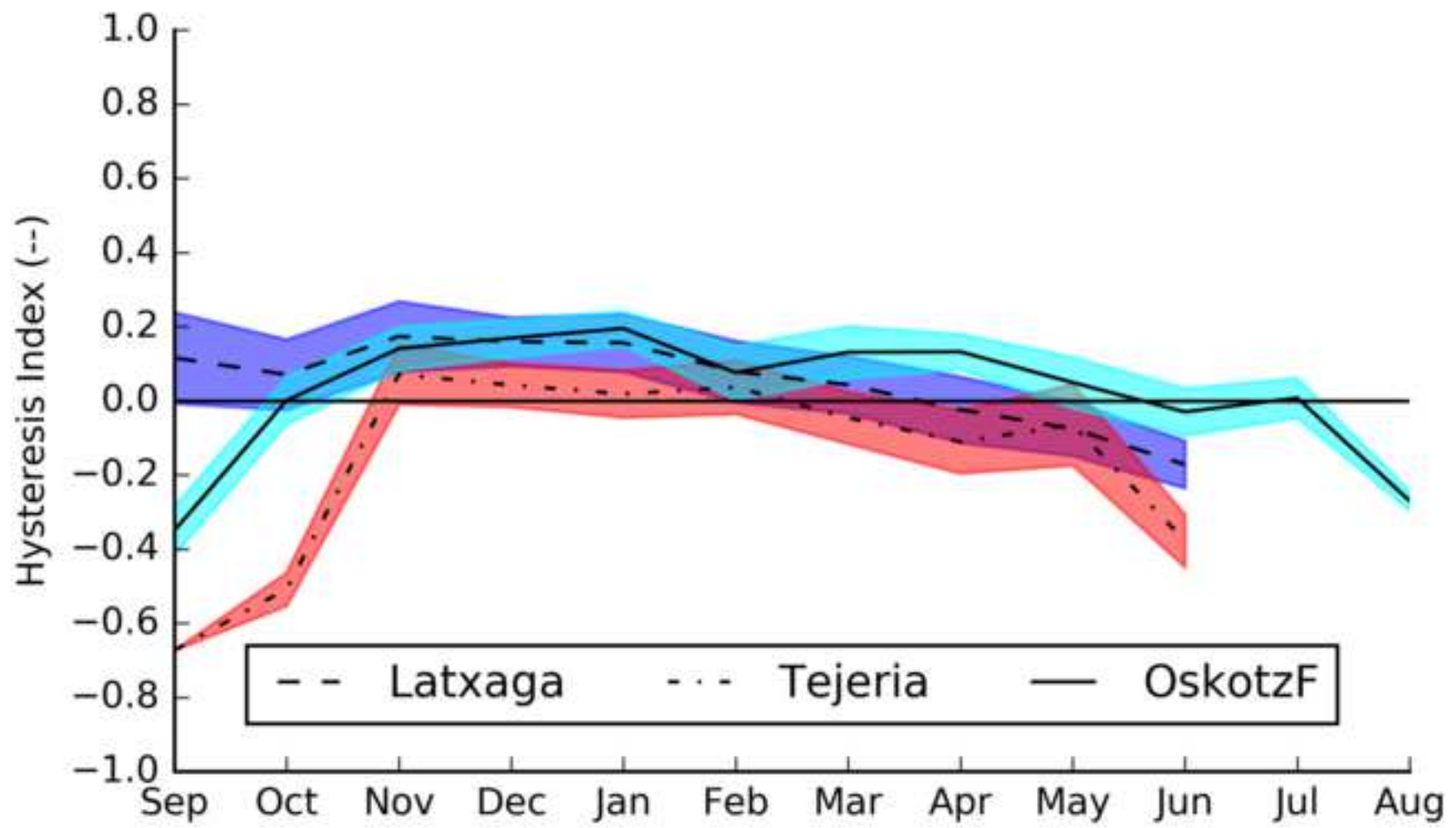
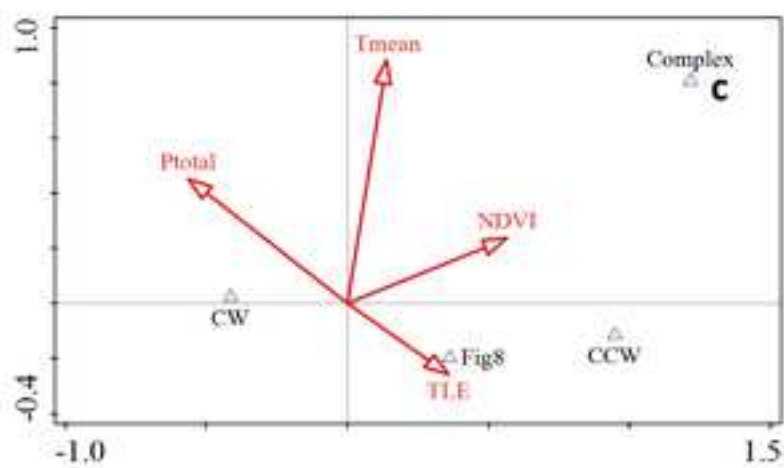
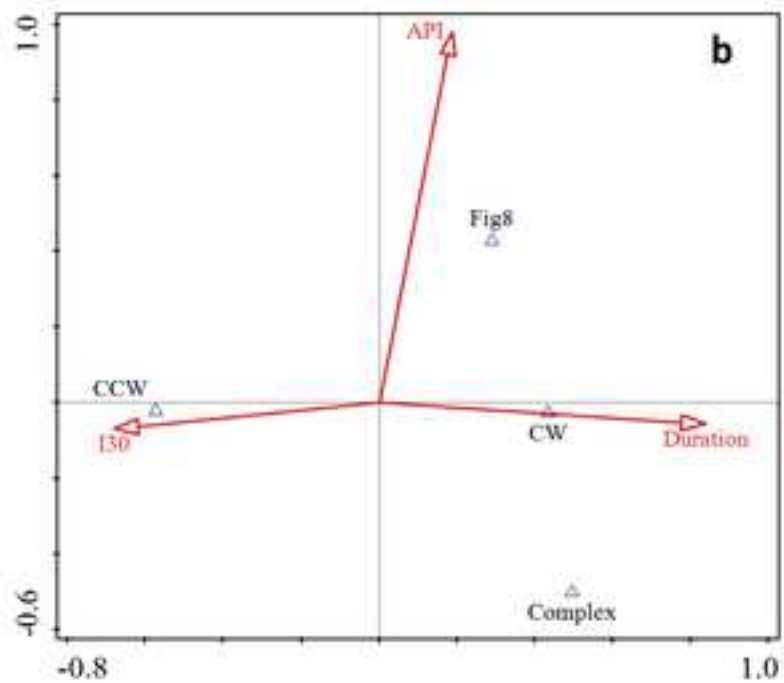
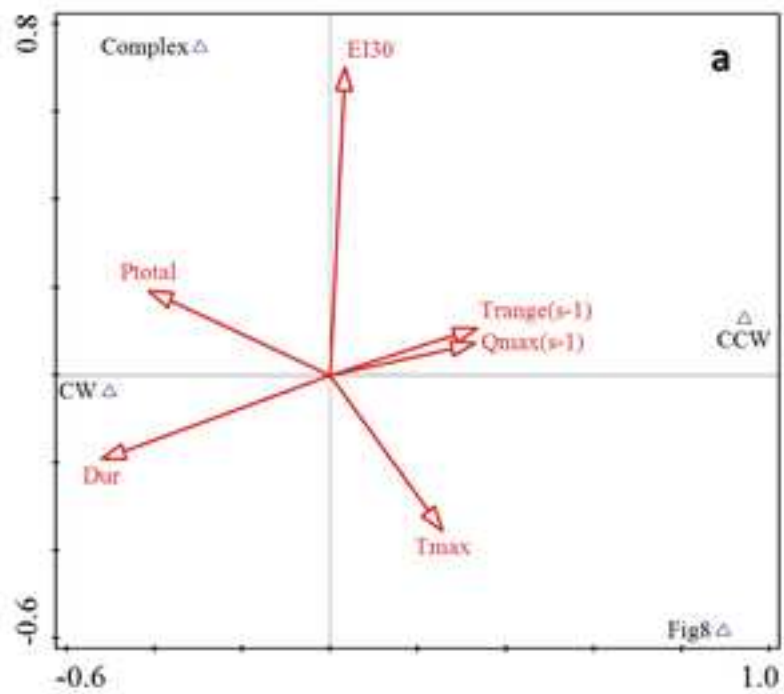


Figure 4





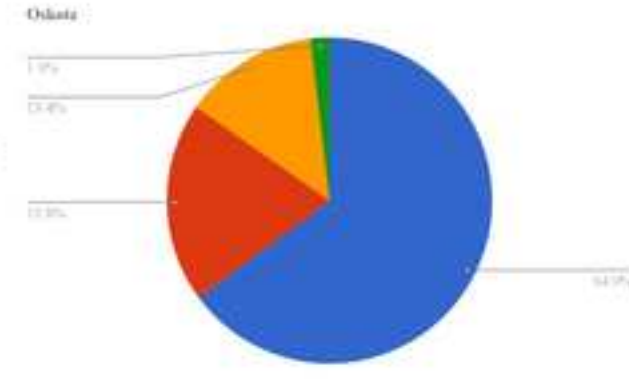
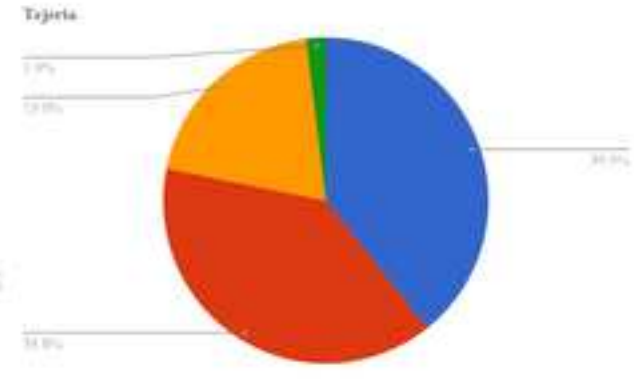
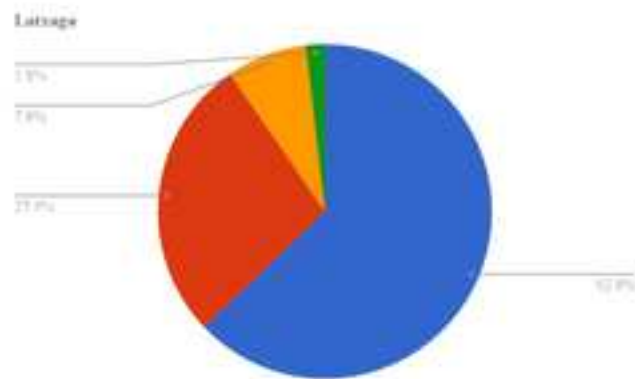
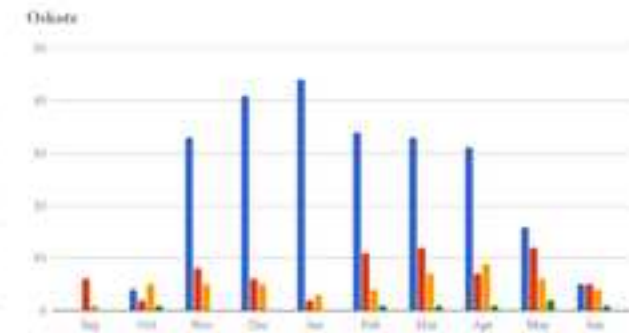
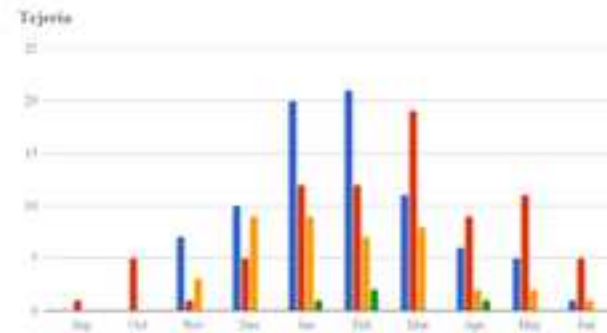
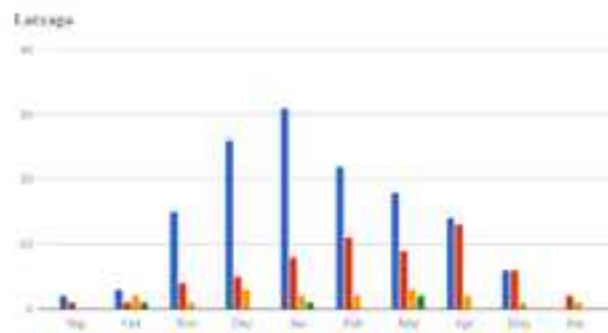


Figure 7: Landscapes of Latxaga (A): complex morphology, riparian vegetation and La Tejeria (B): smooth, little riparian vegetation and bank failures.

